

220-to-320-GHz Fundamental Mixer in 60-nm InP HEMT Technology Achieving 240-Gbps Dual-Band Data Transmission

Teruo Jyo¹, Member, IEEE, Hiroshi Hamada¹, Member, IEEE, Takuya Tsutsumi¹, Member, IEEE, Ibrahim Abdo¹, Member, IEEE, Satoshi Kawahara¹, Member, IEEE, Daisuke Kitayama, Member, IEEE, Munehiko Nagatani¹, Member, IEEE, and Hiroyuki Takahashi¹, Member, IEEE

Abstract—We designed and fabricated a 300-GHz-band fundamental mixer in indium phosphide (InP) high electron mobility transistor (HEMT) technology for 6G wireless communications. We devised a widely split frequency matching network to widen the bandwidth of a resistive mixer. The mixer IC achieved a conversion gain of -15 and -6 -dB RF bandwidth of 100 GHz (220–320 GHz), the widest ever reported. We implemented the mixer IC as a WR3.4 waveguide mixer module and performed a back-to-back data transmission experiment in three different frequency bands. Data rates of 120, 152, and 168 Gbps were achieved in each band. We also developed a dual-band data transmission system with a local oscillator (LO) leakage canceling method. It was capable of transmitting data at 240 Gbps, the highest rate reported to date, and suppressing LO leakage by 60 dB.

Index Terms—Indium phosphide high electron-mobility transistor (InP HEMT), resistive mixer, 6G, 300-GHz band.

I. INTRODUCTION

THE 300-GHz band is expected to be used for high-speed data transmissions in sixth-generation wireless communications (6G). For example, standardization of bands with a maximum bandwidth of 69 GHz from 253 to 322 GHz has been discussed in IEEE 802.15.3d [1]. A 300-GHz-band mixers with a wide RF bandwidth and high linearity are essential components for utilizing such a wide band and achieving a high data rate. Mixers with a wide bandwidth fabricated in indium phosphide (InP) high electron mobility transistor (HEMT), InP heterojunction bipolar transistor (HBT), silicon complementary metal–oxide–semiconductor (CMOS), and silicon-germanium (SiGe) bipolar CMOS (BiCMOS) technologies have been reported [2], [3], [4], [5], [6], [7], [8], [9], [10], [11]. Among them, the resistive mixer [2], [3] has the advantages of having a wide band and high linearity with a simple configuration.

In this work, we designed and fabricated a fundamental resistive mixer in InP HEMT technology. To enlarge the bandwidth of the mixer IC, we devised a widely split

frequency (WSF) matching network. The fabricated mixer IC achieved a conversion gain of -15 , a -3 -dB RF bandwidth of 60 GHz, and a -6 -dB RF bandwidth of 100 GHz, the widest ever reported.

We packaged the mixer IC as a WR3.4 waveguide mixer module. The mixer module had a gain of -16 dB, and it could operate over almost the whole band from 220 to 320 GHz. We used a single mixer module in the TX and in the RX and performed a back-to-back data transmission experiment in three different frequency bands. Data rates of 120, 152, and 168 Gbps were achieved in each band.

As an expansion of our work [12] published in IMS2023, we developed a dual-band data transmission system using two mixers in TX and RX to increase the data rate. To suppress local oscillator (LO) leakage from the TX mixers, we devised an LO canceling method where the phase difference of the LO leakages from the two mixers is adjusted to be 180° and the leakages are canceled at the output. The system could transmit data at 240 Gbps in a back-to-back configuration and suppress LO leakage by over 60 dB.

These results indicate that our mixer is the first one to achieve a data rate over 100 Gbps in multiple frequency ranges in the 300-GHz band. Moreover, the achieved data rate (240 Gbps) is the highest ever reported.

II. TECHNOLOGY

We designed and fabricated the mixer IC with our in-house InP HEMT technology [13]. Fig. 1(a) shows a scanning transmission electron microscope (STEM) image of the area around the gate electrode of the fabricated InP HEMT. The HEMT was grown on a 3-in InP wafer by metal-organic chemical vapor deposition (MOCVD). The gate length (L_g) was around 60 nm. The channel was composed of an 18-nm-thick InGaAs with a mobility of $13\,500\text{ cm}^2/\text{V}\cdot\text{s}$. To reduce the source resistance and improve RF performance, a cap recess region with a length of 150 nm was formed. Fig. 1(b) shows the measured RF performance of the InP HEMT with a gate width (W_g) of $20 \times 2\ \mu\text{m}$ fingers and at a gate voltage of -0.2 V and the drain voltage of 1.2 V . It was measured by a vector network analyzer (VNA) in two bands, from 5 to 125 GHz, and from 220 to 260 GHz. The pads and the lead line to the transistor were de-embedded by using the thru-reflect-line (TRL) method. The maximum oscillation

Manuscript received 9 July 2023; revised 19 September 2023; accepted 11 October 2023. Date of publication 3 November 2023; date of current version 10 January 2024. (Corresponding author: Teruo Jyo.)

The authors are with the NTT Device Technology Laboratories, NTT Corporation, Atsugi 243-0198, Japan (e-mail: teruo.jyo@ntt.com).

Color versions of one or more figures in this article are available at <https://doi.org/10.1109/TMTT.2023.3327478>.

Digital Object Identifier 10.1109/TMTT.2023.3327478

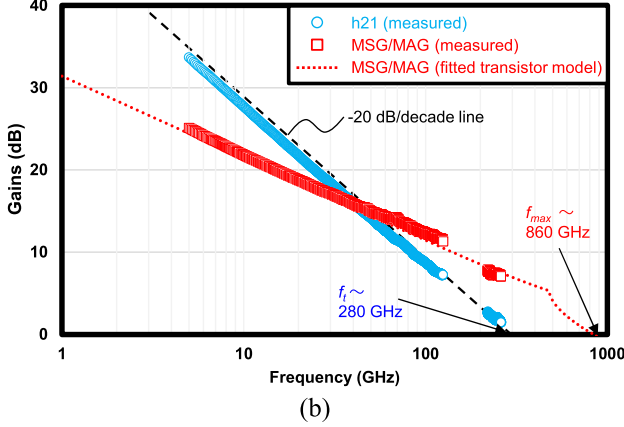
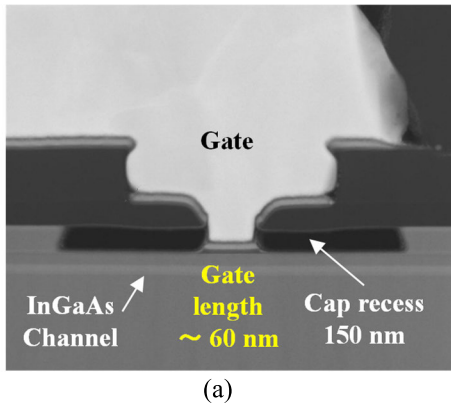


Fig. 1. (a) STEM image and (b) measured RF performance of 60-nm-gate-length InP-HEMT. h21 is short circuit current gain. MSG is the maximum stable gain. MAG is the maximum available gain.

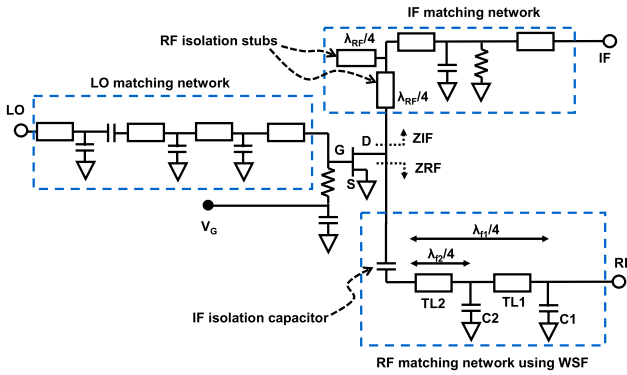


Fig. 2. Schematic of resistive mixer with WSF matching network.

frequency (f_{max}) and the short-circuit current-gain cut-off frequency (f_i) were estimated to be 860 and 280 GHz, respectively.

III. CIRCUIT DESIGN

Fig. 2 shows a schematic of our mixer IC designed using InP HEMT technology. We employed a fundamental resistive mixer for wide-bandwidth and high-linearity operation. In this type of mixer, the transistor is operated as a variable resistor controlled by the gate voltage. By providing a sufficiently large LO power to the gate, the IF/RF signal at the drain is mixed with the LO signal. Since this type of mixer operates like a passive circuit, it is possible to use the same mixer IC for both up-conversion and down-conversion.

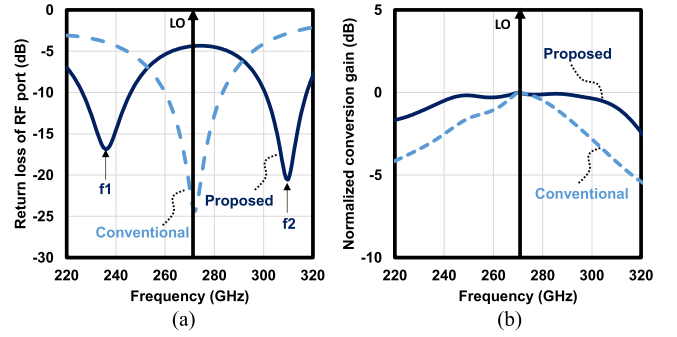


Fig. 3. Simulated (a) return loss of RF port and (b) conversion gain with and without WSF matching network.

To achieve a high conversion gain and wide bandwidth in the resistive mixer, it is important to place matching networks at each port of the LO, IF, and RF. To adapt the mixer to multiple LO frequencies, we designed a broadband LO matching network using multiple matching components such as capacitors and transmission lines. Adding many matching components is generally not desirable because it increases signal loss. However, the loss in the LO matching network is tolerable to some level, since a high-power LO signal is used in the saturation region.

On the other hand, the matching network of the RF port significantly affects the RF bandwidth of the mixer. However, we cannot use many matching components in the RF matching network to widen the bandwidth, unlike the case of the LO matching network. This is because RF power in a practical transmission system must be backed off from the saturation power to maintain its linearity, and the loss in the RF matching circuit directly leads to a reduction in conversion gain. Therefore, the matching frequency of the RF port is generally designed with few matching components to be around the LO frequency, as shown by the dashed line in Fig. 3(a). In this type of matching network, the conversion gain is high around the LO frequency, but decreases away from it, which causes a narrowing of the RF bandwidth.

In this work, we devised a WSF matching network to enlarge the RF bandwidth. Here, the matching frequency of the RF port is not designed to be around the LO frequency, but rather to be close to the edge frequencies of the lower side (f_1) and the higher side (f_2) of the desired band, as shown by the solid line in Fig. 3(a). Only two capacitors, C_1 and C_2 , and two transmission lines, TL_1 and TL_2 , are used to minimize the loss. The impedance at f_1 is basically matched by using TL_1 , TL_2 , and C_1 . The electrical length of these matching components is designed to be $\lambda_{f_1}/4$, where λ_{f_1} is the wavelength of f_1 . The impedance at f_2 is basically matched by using TL_2 and C_2 . The electrical length of these matching components is designed to be $\lambda_{f_2}/4$, where λ_{f_2} is the wavelength of f_2 . The RF characteristics were numerically optimized using electromagnetic field simulations.

Although the WSF matching network causes a little deterioration in the conversion gain near the LO frequency, it avoids a large gain attenuation far from the LO frequency, resulting in a wider bandwidth. The simulation results shown in Fig. 3(b) confirm that the WSF matching network enlarged the

RF bandwidth. For the conventional RF matching network in this figure, we used a circuit similar to Fig. 2 and adjusted each component of the RF matching network to make the matching frequency around 270 GHz.

Another important point when designing the matching network of the resistive mixer is the isolation between the RF signal and the IF signal [3]. To achieve a high conversion gain, the impedance of the RF port side as seen from the drain node of the transistor (ZRF in Fig. 2) should be high in the IF frequency band. Likewise, the impedance of the IF port side as seen from the drain node of the transistor (ZIF in Fig. 2) should be high in the RF frequency band. Here, to increase the isolation, we placed an IF isolation capacitor in the RF matching network and two stubs in the IF matching network with a quarter wavelength in the RF band.

Fig. 4(a) and (b) show simulation results of the ZIF and ZRF. They confirm that ZIF in the RF band is high due to the RF isolation stubs, whereas the ZRF was high due to the IF isolation capacitor. Moreover, the simulation results shown in Fig. 4(c) and (d) illustrate the improvements in the conversion gain and the bandwidth due to these isolation components.

IV. MEASUREMENT RESULTS

A. Mixer IC and Module

Fig. 5(a) shows a photograph of the mixer IC fabricated in our InP HEMT technology. The die size is 1 mm^2 including pads. The power consumption is almost zero, although a very small gate current flows. Fig. 6 shows the setup for measuring the conversion gain of the mixer IC in an on-wafer probing environment. Here, we used a VNA (Keysight N5247A) and a WR3.4 frequency extender. The reflection characteristics of the RF port and LO port were measured with a similar setup. Figs. 7 and 8 show the measured return loss of the LO port and the RF port. For the LO port, a good return loss of less than -10 dB was measured from 230 to 325 GHz. For the RF port, a good return loss of less than -10 dB was measured from 250 to 325 GHz. Our aimed-for split matching frequencies at 260 and 320 GHz were confirmed there. Fig. 9 shows the measured conversion gain of the mixer IC at the LO frequency of 270 GHz. The LO power was around 0 dBm, which was limited by our measurement setup, but was almost in the saturation region. A conversion gain of -15 dB with a -3-dB RF bandwidth of 60 GHz (235–295 GHz) and a -6-dB RF bandwidth of 100 GHz (220–320 GHz) was achieved.

We implemented the mixer IC as a WR3.4 waveguide mixer module for a data transmission experiment. Fig. 5(b) shows a photograph of the module. We used ridge couplers [3], [15] for a smooth mode conversion between the planar mode inside the IC and the waveguide mode of the module. Fig. 10 shows the measured conversion gain of the mixer module at a LO frequency of 270 GHz and LO power of around 7 dBm. The conversion gain was -16 dB with a -3-dB RF bandwidth of 65 GHz (240–305 GHz) and a -6-dB RF bandwidth of 95 GHz (225–320 GHz). Fig. 11 shows the measured output RF power at the LO frequency of 270 GHz, IF frequency of 5 GHz, and RF frequency of 265 GHz. An output 1-dB gain compression point (OP1dB) of -16 dBm was achieved.

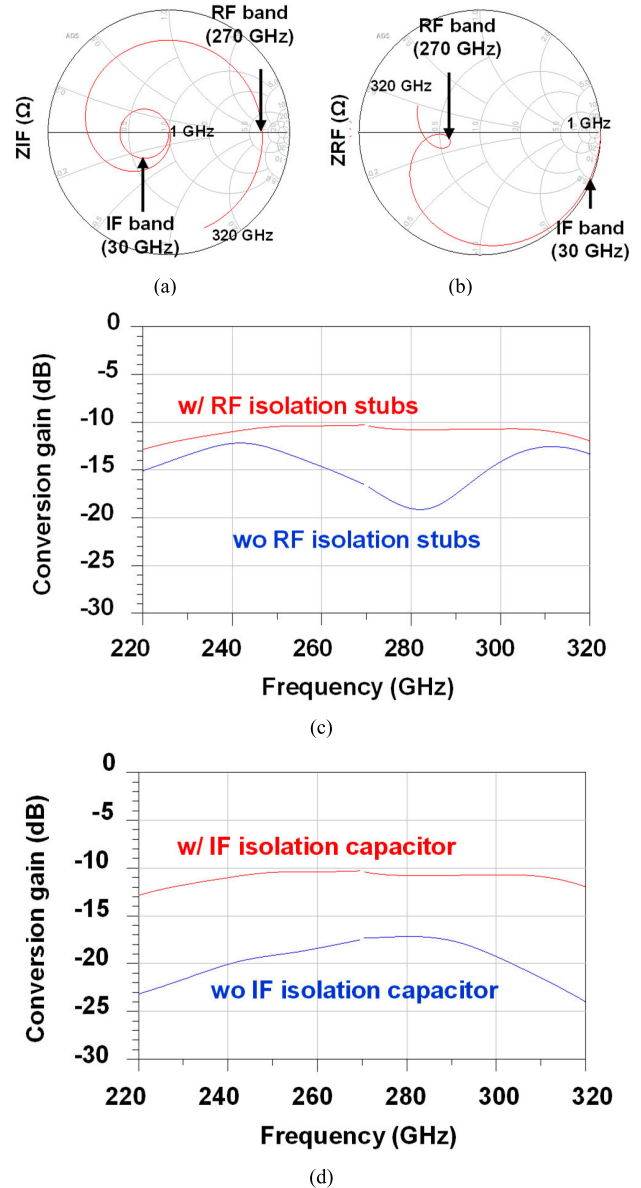


Fig. 4. Simulated impedance of (a) ZIF and (b) ZRF from 1 to 320 GHz. (c) Simulated conversion gain with and without RF isolation stubs. (d) Simulated conversion gain with and without IF isolation capacitor.

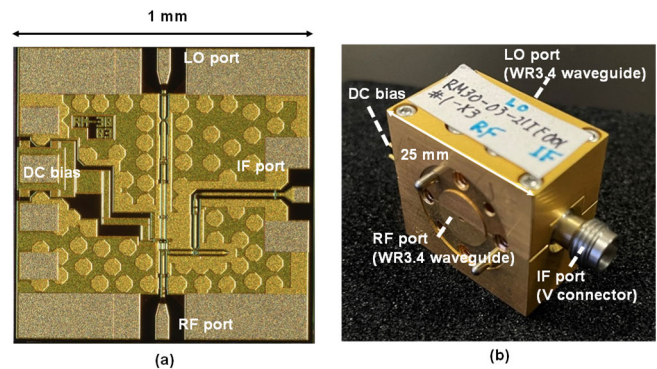


Fig. 5. Photograph of (a) mixer IC and (b) mixer module.

B. Switched Three-Band Data Transmission Experiment

We used one mixer module in the TX and one in the RX for a data transmission experiment in the back-to-

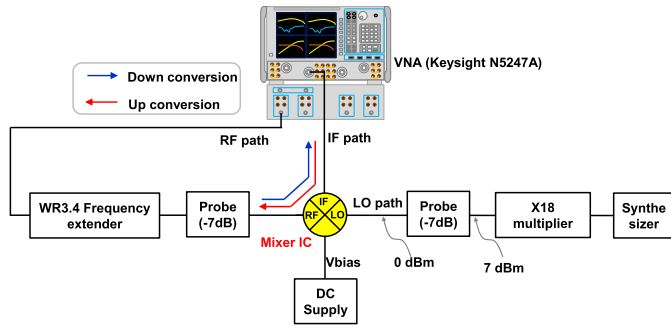


Fig. 6. Setup for measuring conversion gain of mixer IC in the on-wafer probing environment.

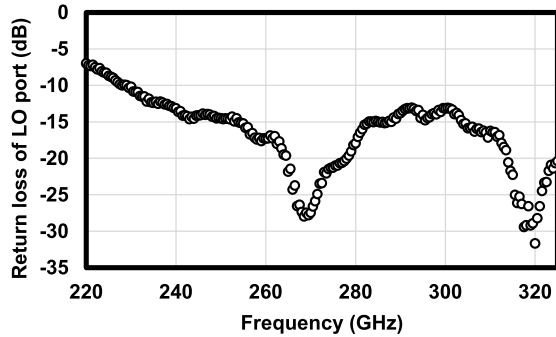


Fig. 7. Measured return loss at LO port of mixer IC.

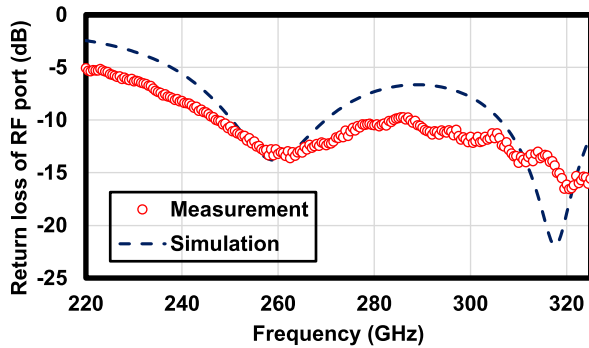


Fig. 8. Measured return loss of RF port of mixer IC.

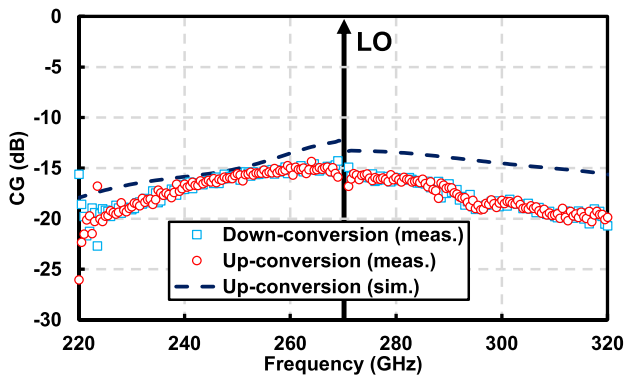


Fig. 9. Measured conversion gain of mixer IC at LO = 270 GHz.

back configuration. The measurement setup is shown in Fig. 12. We used an arbitrary waveform generator (AWG) (Keysight M8199A) to generate an input quadrature amplitude modulation (QAM) IF signal for the TX mixer. The

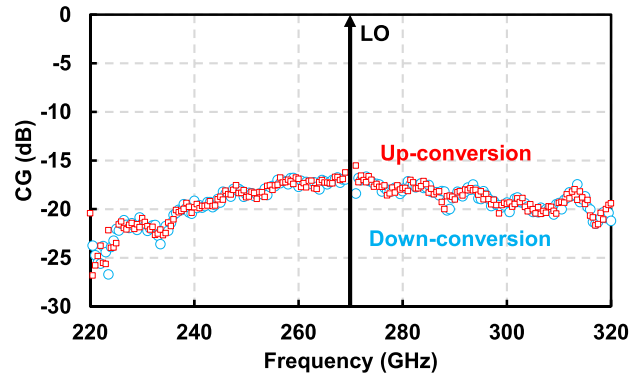


Fig. 10. Measured conversion gain of mixer module at LO = 270 GHz in waveguide measurement environment.

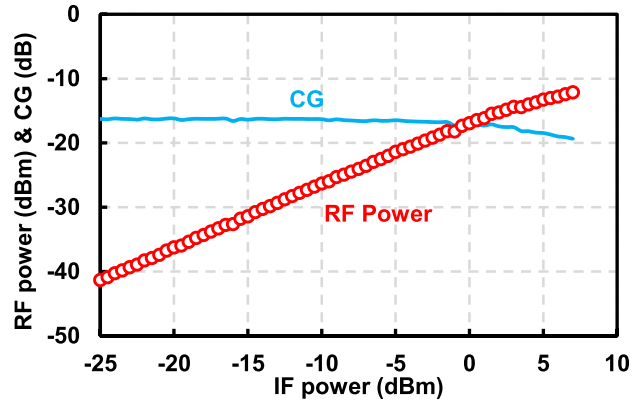


Fig. 11. Measured input and output power characteristics of mixer module at LO = 270 GHz, IF = 5 GHz, and RF = 265 GHz.

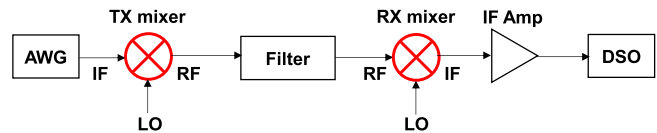


Fig. 12. Measurement setup of back-to-back data transmission experiment.

TABLE I
ALLOCATION OF EACH BAND

	1 st band	2 nd band	3 rd band
LO freq. [GHz]	252.5	282.5	282.5
Filter	Low pass filter (f _{cut} =247.5 GHz)	Low pass filter (f _{cut} =277.5 GHz)	High pass filter (f _{cut} =287.5 GHz)
RF signal center freq. [GHz]	227	257	307
Symbol rate [GBaud]	20	42	38
Modulation format	64 QAM	16 QAM	16 QAM
Occupied frequency range [GHz]	216.5 – 237.5	233.9 – 282.2	284.2 – 329.8
Data rate [Gbps]	120	168	152

output IF signal from the RX mixer was measured using a digital storage oscilloscope (DSO) (Keysight UXR1104A). The experiment was performed in three different frequency bands. The allocation of each band is shown in Table I. We used three different waveguide filters between the TX mixer and the RX mixer to clip each desired band and suppress

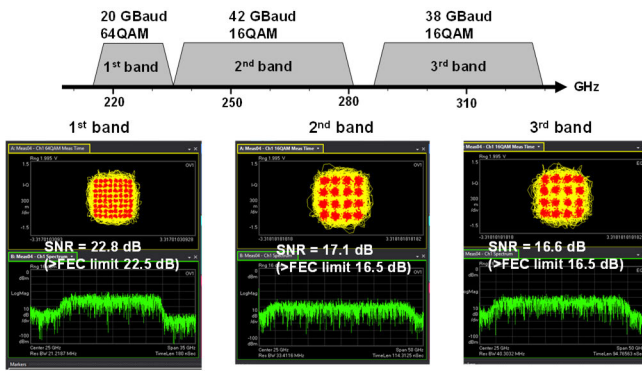


Fig. 13. Measured constellation and spectra of each band in back-to-back data transmission experiment.

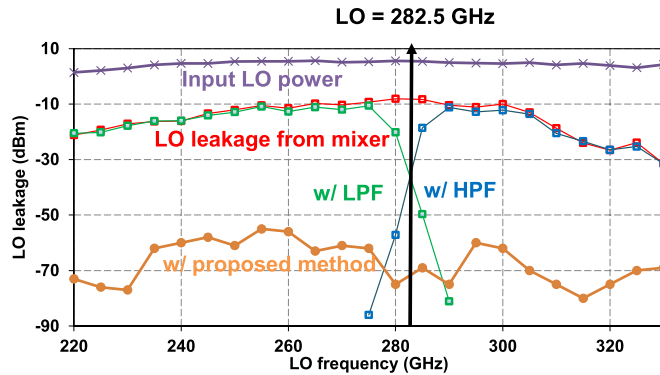


Fig. 14. Measured LO leakage with filters and with the proposed method.

the undesired LO leakage and image signal. Fig. 13 shows the measured constellation and spectrum of the output IF signal of the RX mixer in each of the three bands. In the first band with a center frequency of 227 GHz, a data rate of 120 Gbps (20 GBaud 64 QAM) was achieved with an SNR of 22.8 dB, which is higher than the forward error correction (FEC) limit of 22.5 dB. The FEC limit is the minimum SNR required for errors to be corrected by using the FEC. In the second band with a center frequency of 257 GHz, the data rate was 168 Gbps (42 GBaud 16 QAM) with an SNR of 17.1 dB, which is higher than the FEC limit of 16.5 dB, while in the third band with a center frequency of 307 GHz, it was 152 Gbps (38 GBaud 16 QAM) with an SNR of 16.6 dB, again higher than the FEC limit.

C. Transmitter With LO Canceling Method

LO leakage from the mixer should be suppressed to prevent emissions of unnecessary signals into space from the TX. The fundamental resistive mixer can easily achieve a wide band but has a large LO leakage. Fig. 14 shows the measured LO leakage. The leakage from the mixer module around 282.5 GHz was -10 dBm for an input LO power of 7 dBm. In the data transmission system described in the previous section, waveguide filters were used to suppress the LO leakage. Since the waveguide filters have a limited cutoff characteristic, a guard band from dc has to be set in the IF signal to suppress LO leakage. However, a wide guard band is not desirable because it sacrifices the bandwidth of the IF signal generator, such as an AWG.

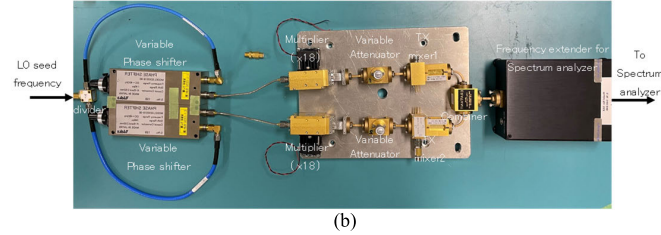
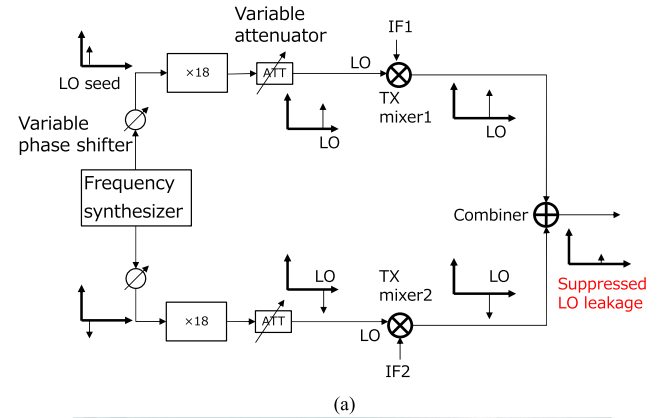


Fig. 15. (a) System block diagram of LO leakage canceling method. (b) Photograph of the measurement system to confirm the effect of LO leak suppression by the proposed method.

The guard band was set to 5 GHz and the LO leakage was suppressed to -35 dBm by using a high pass filter (HPF) or low pass filter (LPF), as shown in Fig. 14 (green line and blue line), which is 25 dB lower than the LO leaking directly from the mixer. The data transmission experiment described in the previous section did not use a power amplifier (PA), but PAs have to be used in a practical wireless communication system after the mixer in order to amplify the signal. For example, if we use a PA with a 20 dB gain, the LO leakage could be amplified to be -15 dBm, which is non-negligible. Therefore, the LO leakage must be further suppressed.

We devised a transmitter system using a LO canceling method for suppressing LO leakage as shown in Fig. 15(a). It uses two mixers are used, and the output is combined by a combiner. By adjusting the LO leakages from the two mixers to be at the same frequency and have the same intensity but opposite phase, they can be canceled when they are combined. The phase of each LO signal is adjusted by using variable phase shifters placed before the frequency multiplier. The intensity of each LO signal is adjusted by variable attenuators placed after the frequency multiplier.

We performed an experiment to confirm the effectiveness of the above LO canceling method. A photograph of the setup is shown in Fig. 15(b). To measure the strength of the LO leakage from the TX, we used a WR3.4 frequency extender and a spectrum analyzer connected to the combiner. The orange line in Fig. 14 shows the results. The LO leakage was substantially suppressed to -70 dBm, which is 60 dB smaller than the LO leakage without the proposed method.

Another advantage of the LO canceling method is that the frequency range of LO leakage suppression is wide; that is, it can be adapted to multiple LO frequencies. Even greater LO leakage suppression can be achieved by additionally using

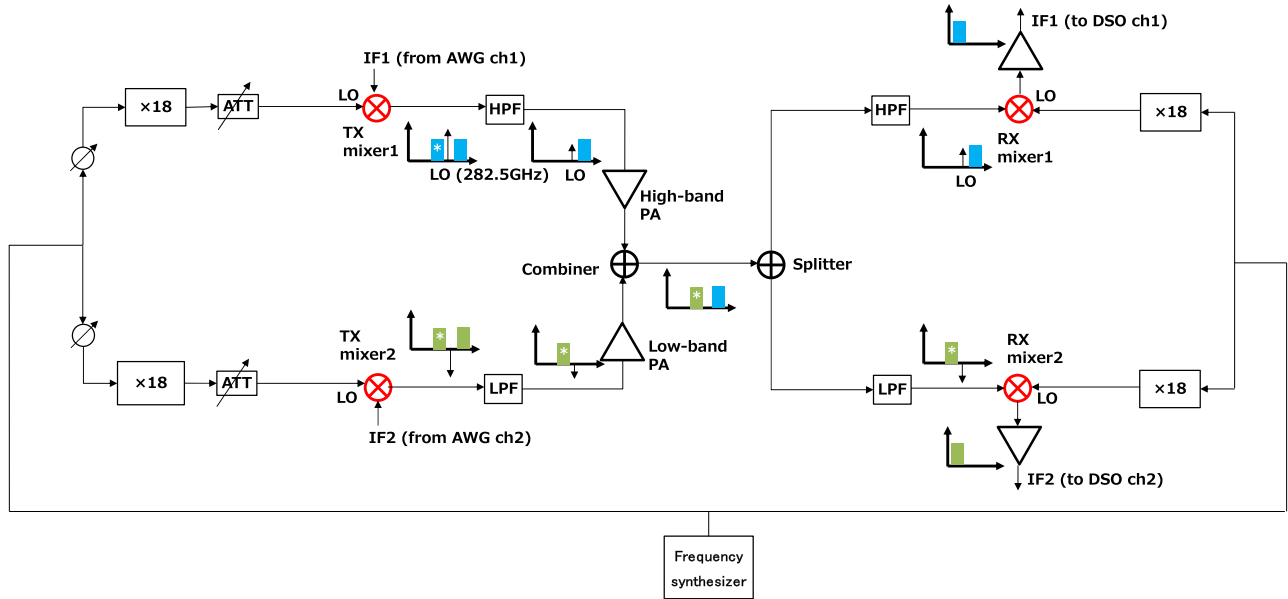


Fig. 16. System configuration of dual-band transmission experiment.

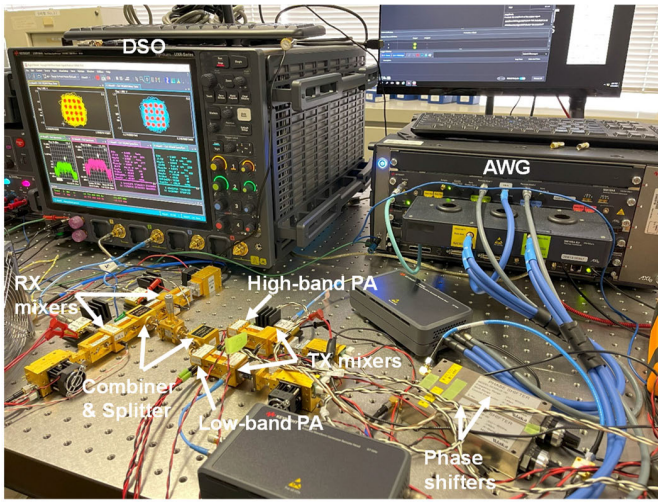
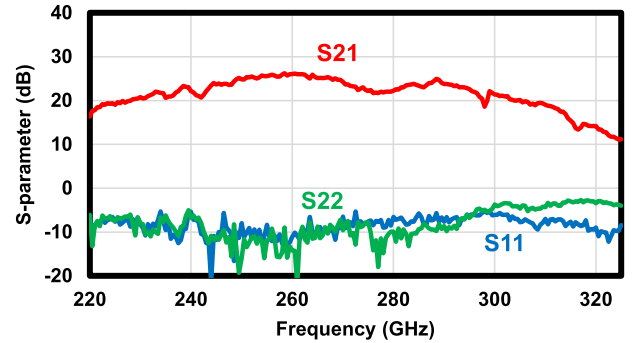


Fig. 17. Photograph of the proposed dual-band data transmission system.

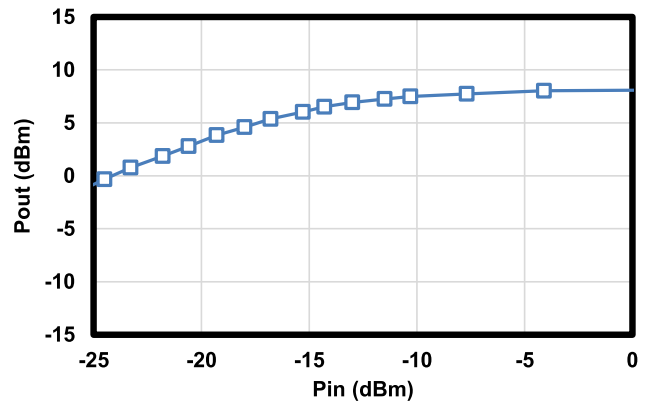
waveguide filters (although no waveguide filter was used in the experiment). Furthermore, as described in the next section, in combination with waveguide filters, the method can perform a dual-band data transmission by inputting different IF data to each mixer.

D. Dual-Band Data Transmission System

We developed a dual-band data transmission system by incorporating the LO canceling method described in the previous section into the transmitter. Figs. 16 and 17 show the block diagram and a photograph of the system. The TX and RX each have two mixers. Two different IF data are input to the TX mixers. An HPF is used to extract the upper side band (high-band) signal from the output of TX mixer1 and an LPF is used to extract the lower side band (low-band) signal from the output of TX mixer2.



(a)



(b)

Fig. 18. Measured (a) S-parameter and (b) power characteristic at 270 GHz of low-band PA.

Two different PA modules, a low-band one and a high-band one, are connected after the filters to amplify the signal in each band. In the low-band PA module, a PA IC that is a modification of the one in [14] is implemented using ridge couplers. Fig. 18(a) shows the measured S-parameter of the low-band PA module. The small signal gain was 24 dB around 270 GHz. Fig. 18(b) shows its measured power characteristic at 270 GHz. The saturation power was

TABLE II
PERFORMANCE SUMMARY AND COMPARISON

Ref	f_{center} [GHz]	-3dB BW (-6dB BW) [GHz]	CG [dB]	OP1dB [dBm]	Technology	Symbol rate [GBaud]	Max. Datarate [Gbps]	IC Implementat ion	Link distance [m]
2	270	32 (50)	-15 (up & down)	-16	80-nm InP HEMT	25 (16QAM)	100	Waveguide module	2.2
3	270	47 (60)	-15 (up & down)	-16.5	80-nm InP HEMT	30 (16QAM)	120	Waveguide module	9.8
4	300	~30 (~50)	-15 (up) -5 (down)	N.A.	250-nm InP-HBT	25 (QPSK)	50	On-board	On-board back-to-back
5	230	26 (30)	16.5 (up) 8 (down)	N.A.	130-nm SiGe BiCMOS	25 (16QAM)	100	On-board	1
6	265	46 (50)	-2 (up) 2 (down)	N.A.	40-nm CMOS	20 (16QAM)	80	Chip with probe	0.03
7	290	26.5 (55)	-19 (down)	N.A.	40-nm CMOS	8 (32QAM)	32	Chip with probe	0.01
8	240	~20 (~30)	-20 (down)	N.A.	65-nm CMOS	26 (QPSK)	52	On-board	0.025
9	135 ($\times 2$)	25 (~35)	-11.4 (up)	-7.5	65-nm CMOS	N.A.	N.A.	N.A.	N.A.
10	265	30 (~35)	26 (down)	N.A.	40-nm CMOS	19 (16QAM)	76	Waveguide module	0.06
11	240	- (35~)	N.A.	N.A.	130-nm SiGe BiCMOS	25 (16QAM)	100	On-board	0.8
This work	270	60 (100)	-15 (up & down)	-16	60-nm InP HEMT	20 (64QAM) @ 1 st band 42 (16QAM) @ 2 nd band 38 (16QAM) @ 3 rd band 32+28 (16QAM) @ dual- band	120 @1 st band 168 @2 nd band 152 @3 rd band 240 @ dual- band	Waveguide module	Waveguide module back-to-back

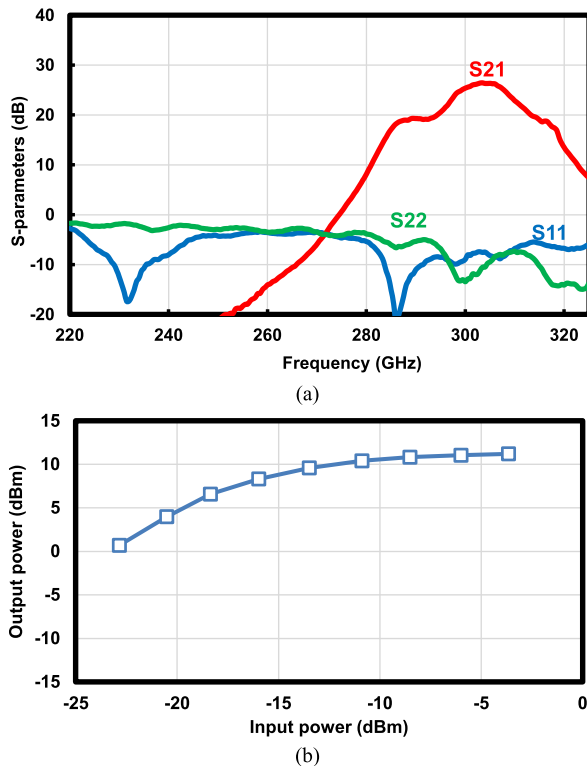


Fig. 19. Measured (a) S-parameter and (b) power characteristic at 270 GHz of high-band PA.

around 8 dBm. The PA IC in the high-band PA module had its frequency tuned from the one in [3]. Fig. 19(a) shows the measured S-parameter of the high-band PA module. The

small signal gain was 25 dB around 300 GHz. Fig. 19(b) shows its measured power characteristic at 270 GHz. The saturation power was around 11 dBm. The combiner after the two PAs combined the signals of the two bands. For LO-leakage cancelling, the LO leakage powers from the two paths can be adjusted to be same level mainly by using the variable attenuators to adjust the LO input powers of the TX mixers. A small adjustment of the LO input power does not have a significant impact on RF power because the mixer operates in the saturation region relative to the LO power. Although the adjustments for the LO leakage canceling were done manually in this study, the system can be made more practical by building an automatic calibration system where the LO leakage power is fed back.

The RX was connected to the TX by using a waveguide in a back-to-back configuration. The RX side used a splitter, HPF, and LPF to split the transmitted two band signals and input them to the two RX mixers. The two IF signals output from the mixers were measured by the DSO at the same time. Fig. 20 shows the measured constellation and spectrum of the IF signals from the RX mixers. The data rate in the high band with a center frequency of 316.5 GHz was 112 Gbps (28 GBaud 16 QAM) with an SNR of 16.7 dB, which is higher than the FEC limit of 16.5 dB. The data rate in the low band with a center frequency of 261 GHz was 128 Gbps (32 GBaud 16 QAM) with an SNR of 18.1 dB, also higher than the FEC limit. The total data rate of the high and low bands was 240 Gbps. Table II summarizes the mixer's performance in comparison with other state-of-the-art 300-GHz-band mixers.

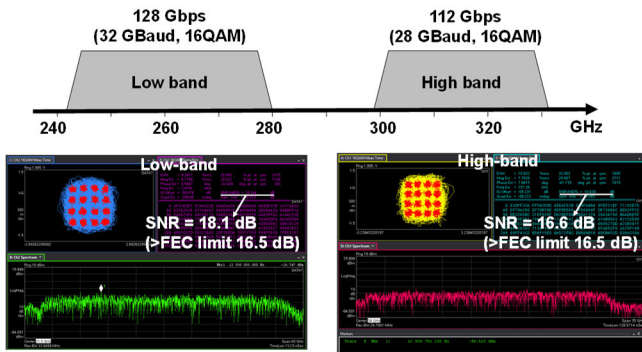


Fig. 20. Measured constellation and spectra of dual-band back-to-back data-transmission experiment.

Our mixer has the widest RF bandwidth, 100 GHz, and the highest data rate, 240 Gbps.

V. CONCLUSION

We designed and fabricated a 300-GHz-band fundamental mixer for 6G wireless communications in InP HEMT technology. To achieve a wide RF bandwidth, we used a resistive mixer and a WSF matching network. The fabricated mixer IC had a conversion gain of -15 dB with a -6 -dB bandwidth of 100 GHz from 220 to 320 GHz, the widest ever reported. We packaged the mixer IC in a mixer module with a WR3.4 waveguide. A single mixer module was used in the TX and in the RX for a back-to-back data transmission experiment in three different frequency bands. Data rates of 120, 152, and 168 Gbps were achieved in each band. We also developed a dual-band data transmission system with a LO leakage canceling method. The system was capable of 240-Gbps data transmissions, the highest rate ever reported, and it suppressed LO leakage by 60 dB.

ACKNOWLEDGMENT

This article is part of the research, “R&D for Expansion of Radio Wave Resources (JPJ000254),” commissioned by The Ministry of Internal Affairs and Communications, Japan.

REFERENCES

- [1] V. Petrov, T. Kurner, and I. Hosako, “IEEE 802.15.3d: First standardization efforts for sub-terahertz band communications toward 6G,” *IEEE Commun. Mag.*, vol. 58, no. 11, pp. 28–33, Nov. 2020, doi: [10.1109/MCOM.001.2000273](https://doi.org/10.1109/MCOM.001.2000273).
- [2] H. Hamada et al., “300-GHz, 100-Gb/s InP-HEMT wireless transceiver using a 300-GHz fundamental mixer,” in *IEEE MTT-S Int. Microw. Symp. Dig.*, Jun. 2018, pp. 1480–1483, doi: [10.1109/MWSYM.2018.8439850](https://doi.org/10.1109/MWSYM.2018.8439850).
- [3] H. Hamada et al., “300-GHz-band 120-Gb/s wireless front-end based on InP-HEMT PAs and mixers,” *IEEE J. Solid-State Circuits*, vol. 55, no. 9, pp. 2316–2335, Sep. 2020, doi: [10.1109/JSSC.2020.3005818](https://doi.org/10.1109/JSSC.2020.3005818).
- [4] H.-J. Song, J.-Y. Kim, K. Ajito, N. Kukutsu, and M. Yaita, “50-Gb/s direct conversion QPSK modulator and demodulator MMICs for terahertz communications at 300 GHz,” *IEEE Trans. Microw. Theory Techn.*, vol. 62, no. 3, pp. 600–609, Mar. 2014, doi: [10.1109/TMTT.2014.2300844](https://doi.org/10.1109/TMTT.2014.2300844).
- [5] P. Rodríguez-Vázquez, J. Grzyb, B. Heinemann, and U. R. Pfeiffer, “A 16-QAM 100-Gb/s 1-M wireless link with an EVM of 17% at 230 GHz in an SiGe technology,” *IEEE Microw. Wireless Compon. Lett.*, vol. 29, no. 4, pp. 297–299, Apr. 2019, doi: [10.1109/LMWC.2019.2899487](https://doi.org/10.1109/LMWC.2019.2899487).
- [6] S. Lee et al., “An 80-Gb/s 300-GHz-band single-chip CMOS transceiver,” *IEEE J. Solid-State Circuits*, vol. 54, no. 12, pp. 3577–3588, Dec. 2019, doi: [10.1109/JSSC.2019.2944855](https://doi.org/10.1109/JSSC.2019.2944855).

- [7] S. Hara et al., “A 32Gbit/s 16QAM CMOS receiver in 300 GHz band,” in *IEEE MTT-S Int. Microw. Symp. Dig.*, Jun. 2017, pp. 1703–1706, doi: [10.1109/MWSYM.2017.8058969](https://doi.org/10.1109/MWSYM.2017.8058969).
- [8] I. Abdo et al., “A bi-directional 300-GHz-band phased-array transceiver in 65-nm CMOS with outphasing transmitting mode and LO emission cancellation,” *IEEE J. Solid-State Circuits*, vol. 57, no. 8, pp. 2292–2308, Aug. 2022, doi: [10.1109/JSSC.2022.3179166](https://doi.org/10.1109/JSSC.2022.3179166).
- [9] Z. Chen, W. Choi, and K. O. Kenneth, “300-GHz double-balanced up-converter using asymmetric MOS varactors in 65-nm CMOS,” *IEEE J. Solid-State Circuits*, vol. 57, no. 8, pp. 2336–2347, Aug. 2022, doi: [10.1109/JSSC.2022.3171545](https://doi.org/10.1109/JSSC.2022.3171545).
- [10] S. Hara et al., “A 76-Gbit/s 265-GHz CMOS receiver with WR-3.4 waveguide interface,” *IEEE J. Solid-State Circuits*, vol. 57, no. 10, pp. 2988–2998, Oct. 2022, doi: [10.1109/JSSC.2022.3179560](https://doi.org/10.1109/JSSC.2022.3179560).
- [11] M. H. Eissa, N. Maletic, E. Grass, R. Kraemer, D. Kissinger, and A. Malignaggi, “100 Gbps 0.8-m wireless link based on fully integrated 240 GHz IQ transmitter and receiver,” in *IEEE MTT-S Int. Microw. Symp. Dig.*, Aug. 2020, pp. 627–630, doi: [10.1109/IMS30576.2020.9224101](https://doi.org/10.1109/IMS30576.2020.9224101).
- [12] T. Jyo et al., “220-to-320-GHz fundamental mixer in 60-nm InP HEMT technology achieving 120/152/168-Gbps data transmission in three bands,” in *IEEE MTT-S Int. Microw. Symp. Dig.*, Jun. 2023, pp. 680–683.
- [13] T. Tsutsumi et al., “Fabrication process technology of InP-based Tera-Hertz ICs for beyond 5G/6G wireless communication networks,” *Compound Semicond. Week (CSW), Semicond. Phys. Division Korean Phys. Soc. (KPS), Seoul, South Korea, Tech. Rep. TuC3-1*, 2023.
- [14] T. Jyo et al., “A 220-294 GHz power amplifier with 10-dBm psat and 2.2% PAE in 250-nm InP DHBT,” in *Proc. IEEE BiCMOS Compound Semiconductor Integr. Circuits Technol. Symp. (BCICTS)*, Oct. 2022, pp. 152–155, doi: [10.1109/BCICTS53451.2022.10051755](https://doi.org/10.1109/BCICTS53451.2022.10051755).
- [15] T. Kosugi et al., “250–300 GHz waveguide module with ridge-coupler and InP-HEMTIC,” in *Proc. Asia-Pacific Microw. Conf.*, Nov. 2014, pp. 1133–1135.



Teruo Jyo (Member, IEEE) received the B.E. and M.E. degrees in electronic engineering from Keio University, Yokohama, Japan, in 2012 and 2014, respectively.

In 2014, he joined the Microsystem Integration Laboratories, Nippon Telegraph and Telephone Corporation (NTT), Atsugi, Japan. He is currently a Researcher with the NTT Device Technology Laboratories, Atsugi, Japan. His research interests are high-speed analog circuit for optical fiber communication and terahertz wave wireless communication

and imaging.

Mr. Jyo received the 2013 IEEE Radio and Wireless Symposium (RWS) Best Student Poster Award, and the 2019 IEEE MTT-S Japan Young Engineer Award.



Hiroshi Hamada (Member, IEEE) received the B.E. and M.E. degrees in electrical engineering from the Tokyo Institute of Technology, Tokyo, Japan, in 2009 and 2011, respectively.

He joined NTT Photonics Laboratories, Nippon Telegraph and Telephone Corporation (NTT), Atsugi, Japan, in 2011. He was engaged in researches of indium phosphide (InP)-transistor-based THz monolithic microwave integrated circuits (MMICs) and modules such as 300-GHz power amplifiers, mixers, transceivers, and 500-GHz amplifiers in NTT Photonics Labs and Device Technology Labs from 2011–2021. He served as an Assistant Manager and a Manager in 6G-IOWN Promotion Department, NTT DOCOMO, Inc., Yokosuka, Japan, from 2021 to 2023. He is currently a Senior Research Engineer at NTT Device Technology Laboratories, Atsugi.

Mr. Hamada is a member of the Institute of Electrical and Electronics Engineers (IEEE) and the Institute of Electronics, Information and Communication Engineers (IEICE). He has been serving as a member of the IEEE Microwave Theory and Technology Society (MTT-S) Technical Committee on Microwave and Millimeter-Wave Solid State Devices (TC-9) since 2021 and ITPC member of the IEEE International Solid-State Circuits Conference (ISSCC) RF Subcommittee since 2023. He was a recipient of the IEEE IMS Best Industry Paper Award in 2016, the URSI AP-RASC Young Scientist Award in 2016, the APMC Prize in 2018, the IEICE Young Researcher’s Award in 2019, the IEEE Excellent Presentation Award in 2022, IEEE MTT-S Japan Young Engineer Award in 2022, and Michiyuki Uenohara Memorial Award in 2022.



Takuya Tsutsumi (Member, IEEE) received the B.E. degree in electrical engineering from Osaka City University, Osaka, Japan, in 2006, and the M.E. and Ph.D. degrees in electronic engineering and informatics from Kyoto University, Kyoto, Japan, in 2008 and 2018, respectively.

In 2008, he joined the NTT Photonics Laboratories, NTT Corporation, Atsugi, Japan. From 2013 to 2016, he was with the NTT Access Network Service Systems Laboratories, NTT Corporation, where he was engaged in the

development of optical network systems. He is currently with the NTT Device Technology Laboratories, NTT Corporation, where he is involved in the research of high-speed indium phosphide-based high-electron-mobility-transistor (InP-HEMT) devices and the development of backside fabrication processes for high-speed ICs.



Ibrahim Abdo (Member, IEEE) received the B.Sc. degree in electronics engineering from Princess Sumaya University for Technology (PSUT), Amman, Jordan, in 2014, and the M.E. degree in physical electronics and the Ph.D. degree in electrical and electronic engineering from the Tokyo Institute of Technology, Tokyo, Japan, in 2017 and 2021, respectively.

He is currently a Researcher with the NTT Device Technology Laboratories, NTT Corporation, Atsugi, Japan, where he is engaged in the research and

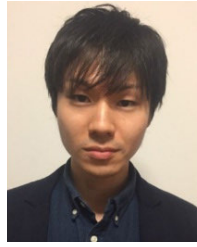
development of monolithic microwave integrated circuits (MMICs) for ultrahigh-speed wireless communications. His research interests include high-data-rate millimeter-wave/sub-terahertz wireless transceiver circuit design and phased-array implementation.

Dr. Abdo was a recipient of the Japanese Government (MEXT) Scholarship and the IEEE SSCS Predoctoral Achievement Award 2021–2022. He serves as a reviewer for IEEE JOURNAL OF SOLID-STATE CIRCUITS (JSSC) and IEEE TRANSACTIONS ON MICROWAVE THEORY AND TECHNIQUES (TMTT).



Satoshi Kawahara (Member, IEEE) received the M.E. degree in electrical and electronic engineering from Kyushu University, Fukuoka, Japan, in 2022.

He joined the NTT Device Technology Laboratories, NTT Corporation, Atsugi, Japan, in 2022, where he is currently engaged in the research on ultrahigh-speed analog ICs for wireline and wireless communications.



Daisuke Kitayama (Member, IEEE) received the B.E. degree in electrical and electronic engineering and the M.E. degree in electronics and applied physics from the Tokyo Institute of Technology, Tokyo, Japan, in 2010 and 2012, respectively.

He joined the NTT Device Technology Laboratories, NTT Corporation, Atsugi, Japan, in 2012. He has been engaged in research on metamaterials for controlling the propagation of terahertz waves. From 2017 to 2021, he has been working as a Research Engineer in 6G Laboratories, NTT

DOCOMO, Inc. and is engaged in research on metasurfaces for fifth- and sixth-generation mobile communication systems. Since May 2021, he has been working as a Senior Research Engineer in NTT Device Technology Laboratories, NTT Corporation, and is involved in research on terahertz metasurfaces for reconfigurable intelligent surface (RIS).



Munehiko Nagatani (Member, IEEE) received the M.S. and Ph.D. degrees in electrical and electronics engineering from Sophia University, Tokyo, Japan, in 2007 and 2021, respectively.

He joined NTT Photonics Laboratories, Atsugi, Japan, in 2007, where he engaged in the research and development (R&D) of ultrahigh-speed analog and mixed-signal ICs for optical communications systems. He is currently with NTT Device Technology Laboratories and NTT Network Innovation Laboratories, where he is involved in R&D of

extreme-broadband ICs for communications and emerging applications.

Dr. Nagatani received the IEICE Young Researcher's Award in 2011, the 67th Maejima Hisoka Encouragement Award in 2022, and the Commendation for Science and Technology by the Minister of Education, Culture, Sports, Science and Technology, the Young Scientists' Award in 2022. He served as a technical program committee (TPC) member for IEEE Compound Semiconductor Integrated Circuits Symposium (CSICS) from 2014 to 2017, and IEEE International Solid-State Circuits Conference (ISSCC) from 2019 to 2023. He has been serving as a TPC member for IEEE BiCMOS and Compound Semiconductor Integrated Circuits and Technology Symposium (BCICTS) since 2018. He is a member of IEICE.



Hiroyuki Takahashi (Member, IEEE) received the B.S. and M.S. degrees in applied physics from Nagoya University, Nagoya, Japan, in 2001 and 2003, respectively, and the Ph.D. degree in advanced electronics and optical science from Osaka University, Osaka, Japan, in 2014.

In 2003, he joined Nippon Telegraph and Telephone (NTT) Microsystem Integration Laboratories, NTT Corporation, Atsugi, Japan. He is engaged in research and development of Millimeter Wave (MMW)/THz monolithic microwave integrated cir-

cuits (MMICs). His other research interests include ultrahigh-speed wireless technologies.

Dr. Takahashi is a member of the IEEE Microwave Theory and Techniques Society (IEEE MTT-S) and the Institute of Electronics, Information and Communication Engineers (IEICE), Japan. He was the recipient of the 2008 Young Engineers Prize presented at the European Microwave Integrated Circuits Conference, the 2009 Radio Achievement Award of the Association of Radio Industries and Businesses, the 2010 Asia-Pacific Microwave Conference (APMC) Prize, the 2012 IEEE Microwave Theory and Techniques Society (IEEE MTT-S) Japan Young Engineer Award and, the 2012 Asia-Pacific Microwave Conference APMC Prize.